metals

MDPI

Article

Numerical Simulation and Experimental Verification of Nickel-Based Superalloy Disc-Shaped Parts Formed by Semi-Solid Thixoforming

Guanfei Xiao [1], Jufu Jiang [2,*] and Ying Wang [3,*]

[1] Science and Technology on Reactor System Design Technology Laboratory, Nuclear Power Institute of China, Chengdu 610213, China; guanfeixiao@163.com
[2] School of Materials Science and Engineering, Harbin Institute of Technology, Harbin 150001, China
[3] School of Mechatronics Engineering, Harbin Institute of Technology, Harbin 150001, China
* Correspondence: jiangjufu@hit.edu.cn (J.J.); wangying1002@hit.edu.cn (Y.W.)

Abstract: Numerical simulation of the thixoforming process of GH4037 nickel-based superalloy disc-shaped components is performed using DEFORM-3D software (Deform V11). The complete numerical simulation process includes three stages in this work: heat transfer to air, heat transfer on the ejector rod, and the semi-solid thixoforming process. The effects of billet placement, billet temperature, and extrusion velocity on the numerical simulation of thixoforming were investigated. Furthermore, some disc-shaped components were produced through thixoforming to verify the results of numerical simulation. The simulation results indicate that horizontal billet placement is beneficial to the thixoforming of the GH4037 part. A higher billet temperature is good for the filling of disc-shaped components, and the formed part is completely filled when the billet temperature is higher than 1360 °C. Higher extrusion velocity leads to lower effective stress of the disc-shaped component. However, high extrusion velocity easily leads to the separation of solid and liquid phases and aggravates the wear and impact of the dies. The experimental results of thixoforming are in good agreement with the results of numerical simulation, and GH4037 nickel-based superalloy disc-shaped components with complete filling and good surface quality are obtained under the optimized process parameters.

Keywords: nickel-based superalloy; semi-solid thixoforming; numerical simulation; experimental verification

Citation: Xiao, G.; Jiang, J.; Wang, Y. Numerical Simulation and Experimental Verification of Nickel-Based Superalloy Disc-Shaped Parts Formed by Semi-Solid Thixoforming. *Metals* **2023**, *13*, 1613. https://doi.org/10.3390/met13091613

Academic Editors: Marcello Cabibbo and Emin Bayraktar

Received: 1 July 2023
Revised: 31 August 2023
Accepted: 11 September 2023
Published: 18 September 2023

1. Introduction

Semi-solid processing is a promising technology for forming parts within the solid–liquid temperature range of alloys [1]. It makes good use of the characteristics of semi-solid metal materials during development and can ensure the quality and mechanical properties of the formed parts [2]. At present, semi-solid processing has been deeply studied and applied in many alloys, such as aluminum alloys [3–6], magnesium alloys [7–10], titanium alloys [11–13], and steels [14–16], but the research on semi-solid forming of nickel-based superalloys is relatively few. Semi-solid processing is a complex forming process involving multiple physical fields, including stress field, strain field, temperature field, and velocity field [17]. These physical fields are affected by the fluidity of alloy material, die temperature, friction coefficient, extrusion speed, and other parameters, resulting in large differences in the semi-solid forming process, which ultimately leads to different microstructures and mechanical properties of the formed components [18]. Due to the complexity and variability of forming parameters, a large number of experiments will lead to material waste and high costs. Reasonable numerical simulation can be used to replace a large number of repeated tests, thereby reducing the cost of human, material, and financial resources [19]. In addition, through numerical simulation, the filling behavior of alloy, the changes in the

velocity field, temperature field, defect field, and stress field of the formed parts during semi-solid forming can be observed. These parameters are difficult to monitor and analyze in the actual forming process. Therefore, reasonable numerical simulation has important guiding significance for the quality control and defect analysis for the semi-solid forming process [20].

The numerical simulation of semi-solid forming is mainly divided into rheoforming numerical simulation and thixoforming numerical simulation. The numerical simulation of rheoforming is mainly for the forming process of semi-solid slurry with a low solid fraction [21], while the numerical simulation of thixoforming is mainly for the forming process of a semi-solid billet with a high solid fraction [22]. The semi-solid forming process has problems such as high temperature and difficulty observing internal changes during the experimental process. Numerical simulation technology can be used to simulate the filling and solidification of semi-solid forming. Through numerical simulation, it is possible to predict the changes in various physical fields of semi-solid billet during the semi-solid process, as well as the locations and types of defects that may occur in components. It has important guiding significance for the optimal process parameter design and scheme optimization of the semi-solid process [23]. Pierret et al. [24] simulated the thixoforming process of steel using Forge2008© software; the results showed that the filling of the part could be clearly seen in the numerical simulation. Wang et al. [25] simulated the thixoforming process of a Al–Cu–Mn–Ti alloy to manufacture parts with a particular shape via AnyCasting software. These simulation results can effectively guide practical experiments. However, there is little research on the semi-solid forming of nickel-based superalloys.

Because of the high semi-solid temperature of the nickel-based superalloy, thixoforming of semi-solid billets with a high solid fraction is easier to realize. In this paper, the nickel-based superalloy GH4037, which is widely used in the domestic aerospace field [26], was taken as the research object. The numerical simulation of semi-solid thixoforming was carried out, and the influences of different parameters on the forming process were analyzed. Then, the actual thixoforming experiments of GH4037 alloy were carried out to verify the accuracy of the numerical simulation results. It can not only verify the feasibility of forming experiments but also optimize the forming parameters, simplify the actual experimental process, and reduce the experimental cost.

2. Pretreatment of Numerical Simulation of Semi-Solid Thixoforming

The part for semi-solid thixoforming in this work is a disc-shaped turbine disk scaled component, and its two-dimensional diagram and outline dimensions are shown in Figure 1a. UG NX 12.0 software was used to conduct 3D solid modeling of the starting billet and the forming dies. Figure 1b shows the 3D solid model of the disc part; Figure 1c presents the assembly drawing of the forming dies. The die model used for numerical simulation includes three parts: a top die, a bottom die, and an ejector rod. The solid models of dies and billets were saved as ".STL" files and then imported into Deform-3D software.

The billet (Ø35 mm × 52.5 mm) and dies were meshed, and the mesh generation results are shown in Figure 2. The relative grid division method was adopted for meshing the top die, bottom die, and ejector rod. The grid in the region where the die and the billet directly contacted was smaller, while the grid size in other positions was relatively large. The number of grids for the top die, the bottom die, and the ejector rod was 80,000, 45,000, and 50,000, respectively. As for the billet, it was meshed by the absolute grid division method; the minimum grid size was 0.4 mm, and the number of grids was 100,000.

As there is no material model of the GH4037 alloy in the semi-solid temperature range in the material library of Deform-3D software, a new material model of the GH4037 alloy is required. The author previously carried out a semi-solid compression test of the GH4037 alloy [27] and obtained the stress–strain curves of the GH4037 alloy in the semi-solid temperature range. The obtained compression stress–strain curves were imported into Deform-3D software and then the corresponding thermodynamic parameters and

deformation parameters were imported to establish a new material model of the GH4037 alloy. Figure 3 shows the microstructures of the GH4037 alloy. As shown in Figure 3a, the starting material was composed of uniformly distributed equiaxed grains with an average grain size of 28 mm. When the GH4037 billet was heated to 1360 °C, the microstructure exhibited obvious semi-solid structural characteristics. It contained solid phases (solid grains) and liquid phases (liquid droplet and eutectic phase). Additionally, the average grain size increased to 205 mm. At the same time, it was observed that the distribution of solid and liquid phases was relatively uniform at semi-solid temperature. Therefore, in this work, the billet was treated as a homogeneous material.

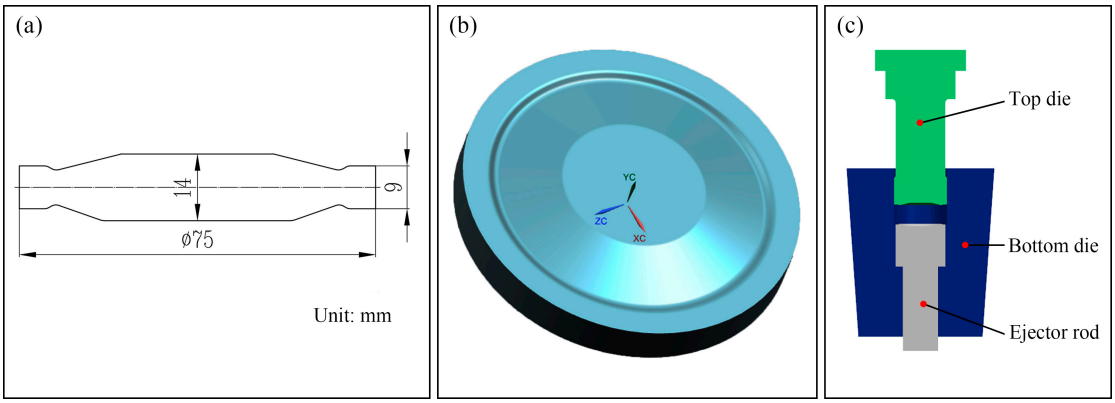

Figure 1. Schematic diagram of the formed part and assembly diagram of dies. (**a**) Two-dimensional drawing of the formed part; (**b**) three-dimensional model of the formed part; (**c**) assembly drawing of the forming dies.

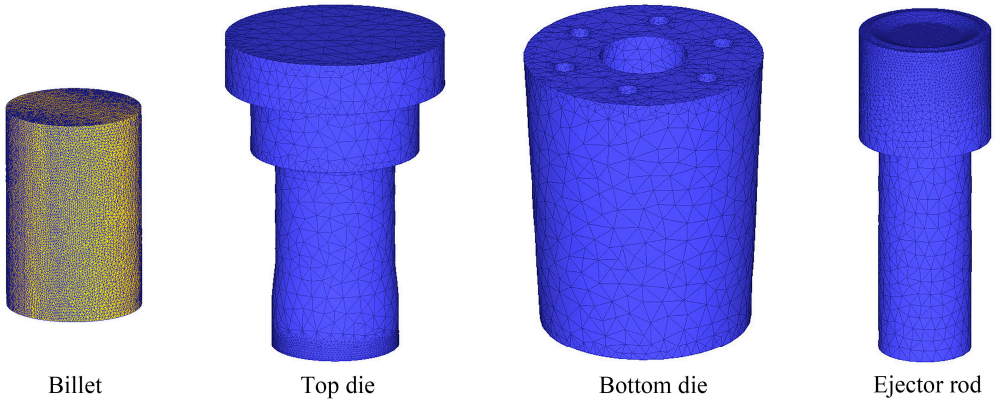

Figure 2. Mesh generation models of the billet, top die, bottom die, and ejector rod.

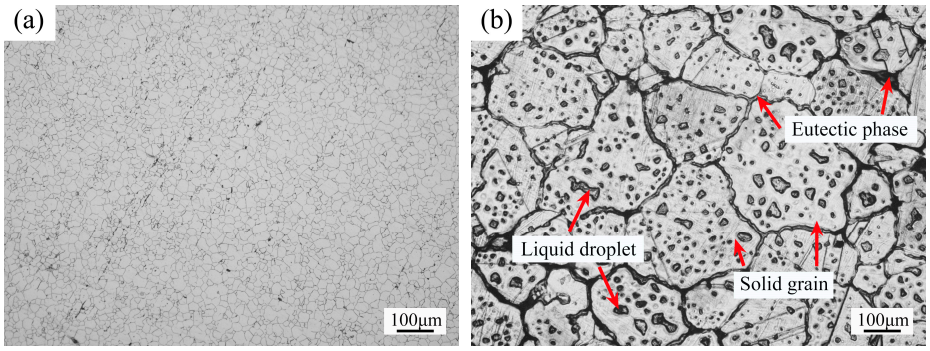

Figure 3. Microstructures of the GH4037 alloy. (**a**) The starting material; (**b**) the billet heated to 1360 °C.

In order to ensure as much consistency between the numerical simulation and experimental process as possible, the numerical simulation of the semi-solid processing of the GH4037 alloy was divided into three steps in this paper:

(1) Transfer process: This process simulated the transfer of the billet from the heating furnace to the mold cavity after heating. In the actual experiment, there was a transfer process after the billet was heated. During the transfer process, the billet transferred heat to air. Therefore, this process should not be ignored. In this work, the transfer time was set to 2 s, the air temperature was 25 °C, and the heat transfer coefficient was 0.02 kW/(m^2·K).

(2) Contact process: This step simulated the process that the billet stayed in the die cavity before being extruded. In this process, the billet directly contacted the upper surface of the ejector rod for heat transfer. The contact time was set to 2 s, and the heat transfer coefficient was 1 kW/(m^2·K).

(3) Thixoforming process: The billet was compressed under the pressure of the top die and then filled the entire mold cavity. In this step, the friction coefficient between the die and billet was set to 0.3, the temperature of the top die was 400 °C, the temperature of the bottom die, the ejector rod temperature was 450 °C, and the heat transfer coefficient was 11 kW/(m^2·K).

The process parameters considered in the numerical simulation mainly include the billet placement mode, billet temperature, and extrusion velocity. The specific experimental parameters are shown in Table 1.

Table 1. Simulation parameters of the semi-solid thixoforming process.

Number	Billet Temperature (°C)	Extrusion Velocity (mm/s)	Billet Placement Mode
1	1380	15	Horizontal
2	1380	15	Vertical
3	1250	15	Horizontal
4	1300	15	Horizontal
5	1350	15	Horizontal
6	1360	15	Horizontal
7	1370	15	Horizontal
8	1380	5	Horizontal
9	1380	10	Horizontal
10	1380	20	Horizontal

3. Results and Discussion

3.1. The Process of Heat Transfer between the Billet and Air

The initial temperature of the semi-solid billet was 1380 °C. The temperature field distribution of the billet after 2 s transfer in air is shown in Figure 4. It can be seen that there was almost no decrease in the maximum temperature of the billet during the transfer process. The surface temperature of the billet was reduced. The lowest temperature appeared at the upper and lower circumferential positions of the billet, which was 1299.2 °C, and the maximum temperature drop was 80.8 °C. Figure 4b shows the temperature field distribution of the billet section. It can be seen that the temperature at the center of the billet had almost no change, and the temperature gradually decreased from the center to the surface. The lowest temperature appeared at the outermost end of the upper and lower circumference.

3.2. The Process of Heat Transfer between the Billet and the Ejector Rod

When the billet was placed on the ejector rod, the top die started to go down, and the billet was in contact with the ejector rod for a period of time before the top die came into contact with the upper surface of the billet. For the accuracy of the numerical simulation of the whole process, the heat transfer between the billet and the ejector rod should also

be considered. In this work, the contact time between the billet and the ejector rod was set as 2 s, the heat transfer coefficient was set as 1 kW/(m^2·K), the initial temperature of the ejector rod was set as 450 °C, and the initial temperature field distribution of the billet was the result in Section 3.1. Because the placement mode of the billet affected the contact area between the billet and the ejector rod, a comparative analysis was carried out in the simulation. The schematic diagram of the horizontal placement of the billet is shown in Figure 5a, and the schematic diagram of the vertical placement of the billet is shown in Figure 5d. First, the heat transfer of the billet in horizontal placement was simulated, and the results are shown in Figure 5b,c. It can be found that when the billet was placed horizontally, the contact position between the billet and ejector rod was two contact points (as shown in the red circles in Figure 5b), and there was a significant temperature change at these two points. The temperature at the contact point of the billet decreased significantly, which was 1248.1 °C, while the temperature at the contact point of the ejector rod increased slightly, which was 464.1 °C. When the billet was placed vertically, the simulation results are shown in Figure 5e,f. It can be seen that when the billet was placed vertically, the whole bottom surface of the billet was completely in contact with the ejector rod, so there was obvious heat transfer at the location of the contact surface. As shown in Figure 5e, the temperature of the contact surface of the billet was significantly reduced, and the temperature of 1216.3 °C at the circumference of the bottom surface was the lowest. As shown in Figure 5f, the temperature at the contact surface of the ejector rod was also significantly increased, and the temperature of 563.2 °C at the center was the highest.

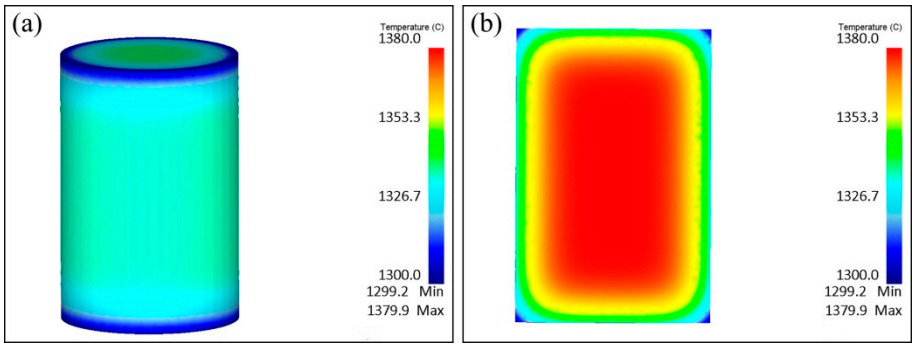

Figure 4. Temperature field of the billet after heat transfer to air. (**a**) The whole billet; (**b**) the billet section.

3.3. Numerical Simulation of the Semi-Solid Thixoforming Process

3.3.1. The Effect of Billet Placement Mode on the Results of Numerical Simulation of Thixoforming

It should be pointed out that the numerical simulation here was followed by Section 3.2. The billets were placed horizontally and vertically, respectively. The temperature of the top die was set as 400 °C, the temperature of the bottom die and ejector rod was set as 450 °C, the friction coefficient was 0.3, and the extrusion velocity of the top die was 15 mm/s. Figure 6 shows the filling process of the billets in different placement modes. As shown in Figure 6a, when the billet was placed horizontally, it first flowed along the axial direction to both ends when extruded. As the two end faces contacted the mold cavity, the billet flowed along the circumference, and finally, the entire forming process was completed. As shown in Figure 6b, when the billet was placed vertically, the upper and lower end faces were extruded, and the billet was not constrained in the circumferential direction, so it flowed freely first. When the billet contacted the side wall of the bottom die, other positions continued to be supplemented, and finally, the entire part was filled.

Figure 7 illustrates the distributions of the temperature field, equivalent strain field, and defect field of the formed parts with different billet placement modes. Due to the different flow conditions when the billets were placed horizontally and vertically, the distribution laws of the physical fields were also different. By comparing Figure 7a,d, it

can be seen that the overall temperature of the formed part was lower when the billet was placed horizontally. So, more plastic deformation could be generated during the forming process, which was conducive to improving the performance of the formed part [28]. As shown in Figure 7d, when the billet was placed vertically, the temperature distribution of the formed part was uniform, the temperature drop was relatively small, and the temperature in most areas was in the semi-solid temperature range, which was beneficial to the smooth filling of the billet. As shown in Figure 7b, the maximum equivalent strain at the edge of the formed part is 2.70, and the average equivalent strain was 0.99. As shown in Figure 7e, the maximum equivalent strain at the inner edge of the formed part was 2.34, but the average equivalent strain was 1.13. As shown in Figure 7c, when the billet was placed horizontally, the defect field was distributed unevenly around the circumference. In Figure 7f, when the billet was placed vertically, the defect field was distributed evenly around the circumference, while the possibility of forming defects was higher because of greater deformation.

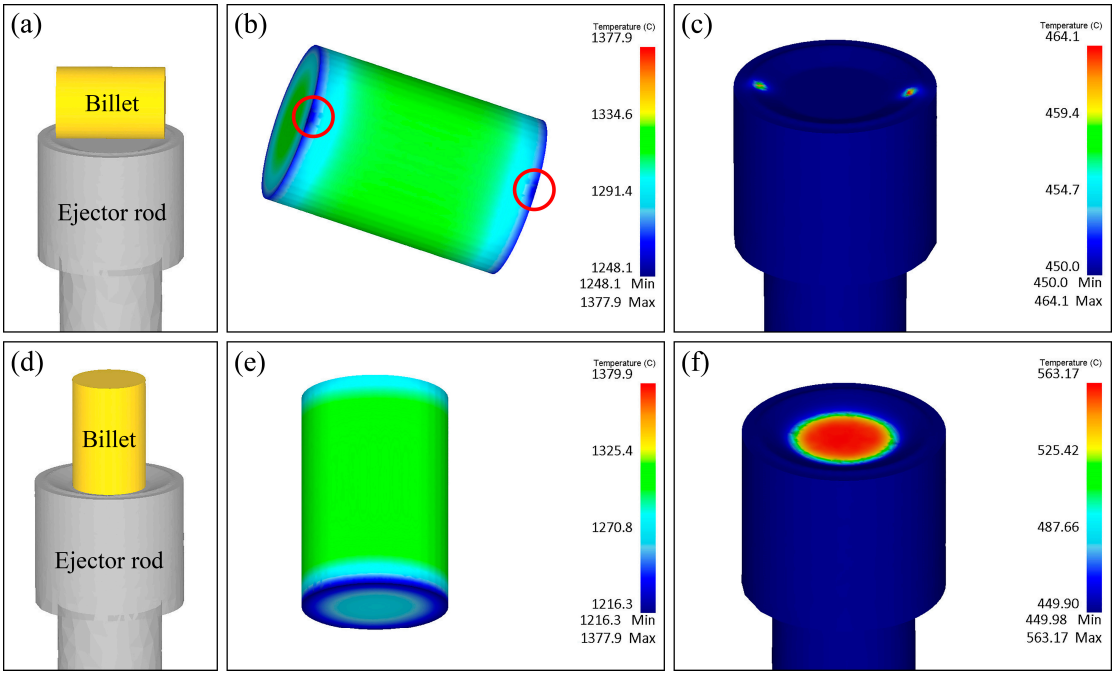

Figure 5. Schematic diagrams of billet placement and temperature distributions of the billet and the ejector after the billet was placed on the ejector for 2 s. (**a**) Schematic diagram of horizontal placement of the billet; (**b**) temperature distribution of the billet as the billet placed horizontally; (**c**) temperature distribution of the ejector as the billet placed horizontally; (**d**) schematic diagram of vertical placement of the billet; (**e**) temperature distribution of the billet as the billet placed vertically; (**f**) temperature distribution of the ejector as the billet placed vertically.

Figure 8 shows the temperature field distributions of the dies with different billet placement modes. Figure 8a–c shows the temperature field distribution of the top die, ejector rod, and bottom die when the billet was placed horizontally. It can be seen that when the billet was placed horizontally, due to the uneven flow of the billet, the mold temperature distribution was also nonuniform. The highest temperature of the top die was 783 °C, the highest temperature of the ejector rod was 806 °C, and the highest temperature of the billet was 694 °C. Figure 8d–f shows the temperature field distribution of the top die, ejector rod, and bottom die when the billet was placed vertically. As the billet flowed uniformly along the circumference during the forming process, the temperature field distribution of the dies was also distributed along the circumference. As shown in Figure 8d–f, the highest temperatures of the top die, ejector rod, and bottom die were 795 °C, 831 °C, and 586 °C, respectively. By comparison, it can be found that the maximum temperatures of

the top die and ejector rod were lower when the billet was placed horizontally than when it was placed vertically. This is mainly because when the billet was placed horizontally, the deformation of the billet in the vertical direction was smaller, and the heat transfer time between the billet and the dies was less with the same extrusion velocity. When the billet was placed vertically, the billet filled the circumferential position at last, so the die temperature was lower.

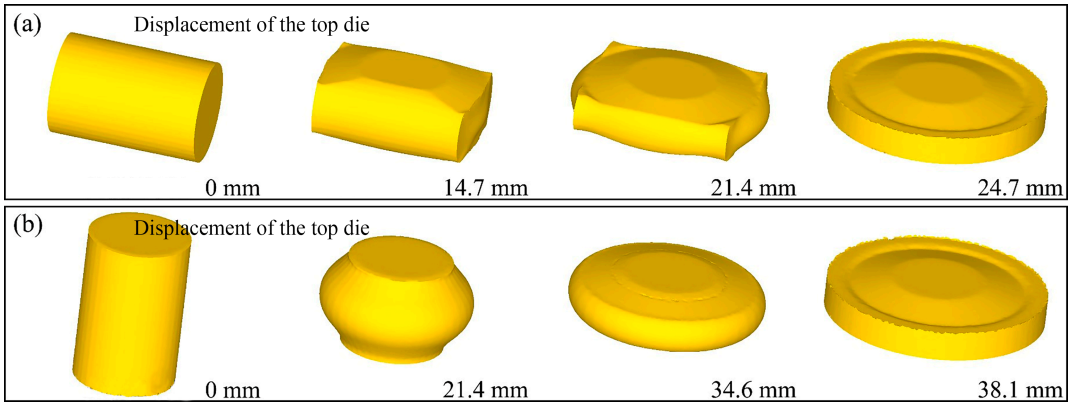

Figure 6. The forming process of the billet with different placement modes. (**a**) Horizontal placement; (**b**) vertical placement.

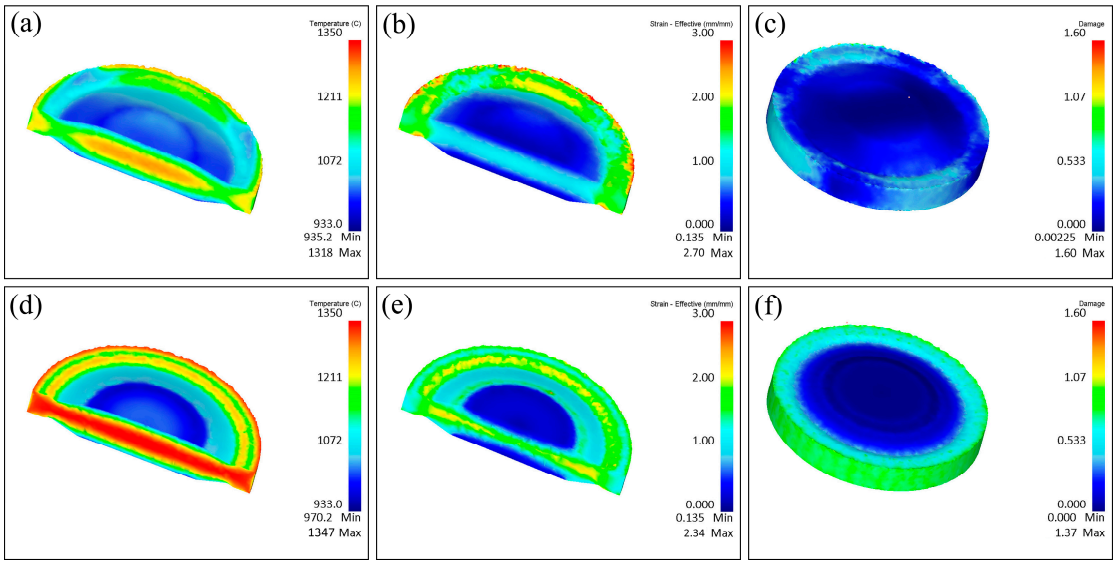

Figure 7. Simulation results of the billets with (**a**–**c**) horizontal placement mode and (**d**–**f**) vertical placement mode. (**a**,**d**) Temperature field; (**b**,**e**) effective strain field; (**c**,**f**) damage field.

By comparing the billet temperature field, equivalent strain field, defect field, and mold temperature field, when the billet was placed horizontally and vertically, the following results were obtained. The die cavity was unevenly filled with billet material when the billet was placed horizontally, while it was evenly filled along the circumference when the billet was placed vertically. However, the die cavity could be completely filled in both ways. Compared with the vertical billet placement mode, when the billet was placed horizontally, the maximum temperatures of the forming part, top die, and ejector rod were lower, while the maximum temperature of the bottom die was higher. Because the temperatures of the top die and ejector rod were higher when the billet was placed vertically, the thermal damage to the dies was also greater. Although the maximum equivalent strain of the billet placed horizontally was higher than that placed vertically, the average equivalent strain

was lower, and the overall deformation of the billet was better. When the billet was placed vertically, the circumferential position was the last filling position, where defects were easy to appear, so the possibility of defects in the formed parts was greater. When placed horizontally, the billet was compressed from 35 mm to 14 mm, and the deformation was 60%. When placed vertically, the billet was compressed from 52.5 mm to 14 mm, and the deformation was 73.3%. As the billet was placed vertically, the deformation was greater, so the defects in the actual forming process were more likely to be generated. From the above results, it can be seen that the horizontal placement mode was more conducive to the thixoforming of the billet, so in the subsequent numerical simulation, the billet was placed horizontally.

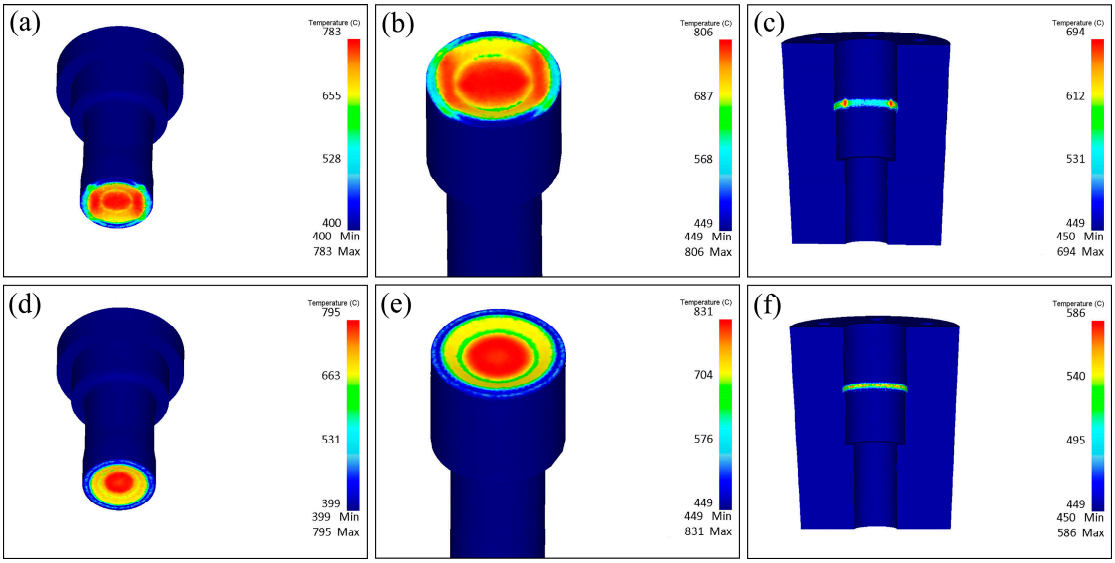

Figure 8. Temperature distributions of the dies with (**a**–**c**) horizontal billet placement mode and (**d**–**f**) vertical billet placement mode. (**a**,**d**) Top die; (**b**,**e**) ejector rod; (**c**,**f**) bottom die.

3.3.2. The Effect of Billet Temperature on the Results of Numerical Simulation of Thixoforming

Figure 9 shows the three-dimensional morphologies of the formed parts with different billet temperatures. As shown in Figure 9a–c, when the billet temperatures were 1250 °C, 1300 °C, and 1350 °C, the outer edge of the formed parts was not completely filled (as shown in the red dotted box in Figure 9). As shown in Figure 9d–f, when the billet temperatures were 1360 °C, 1370 °C, and 1380 °C, the formed parts were completely filled. The simulation results indicated that the billet temperature had a significant effect on the filling performance of the formed parts. When the billet temperature was high enough, the flow performance of the formed part was good, and the formed part could be completely filled.

Figure 10 presents the temperature field distribution of the formed parts with different billet temperatures. It can be found that the temperature distribution of the formed part was roughly similar at different temperatures. The heat transfer at the center of the formed part was slow, so the temperature was the highest. Because the outer edge of the formed part contacted the mold cavity last, the temperature took second place. Since the upper surface of the formed part was always in contact with the top die, there was more heat transfer, and the temperature was the lowest. Meanwhile, it can be found that the highest temperature of the formed parts gradually increased with the increase of the billet temperature. Due to the low temperature of the dies, there was a large heat transfer between the billet and the dies during the forming process, so the final temperature of the formed part dropped significantly, which was basically lower than the solidus temperature. As shown

in Figure 10f, when the billet temperature was high enough (1380 °C), the temperature of some areas of the formed part was still in the semi-solid temperature range.

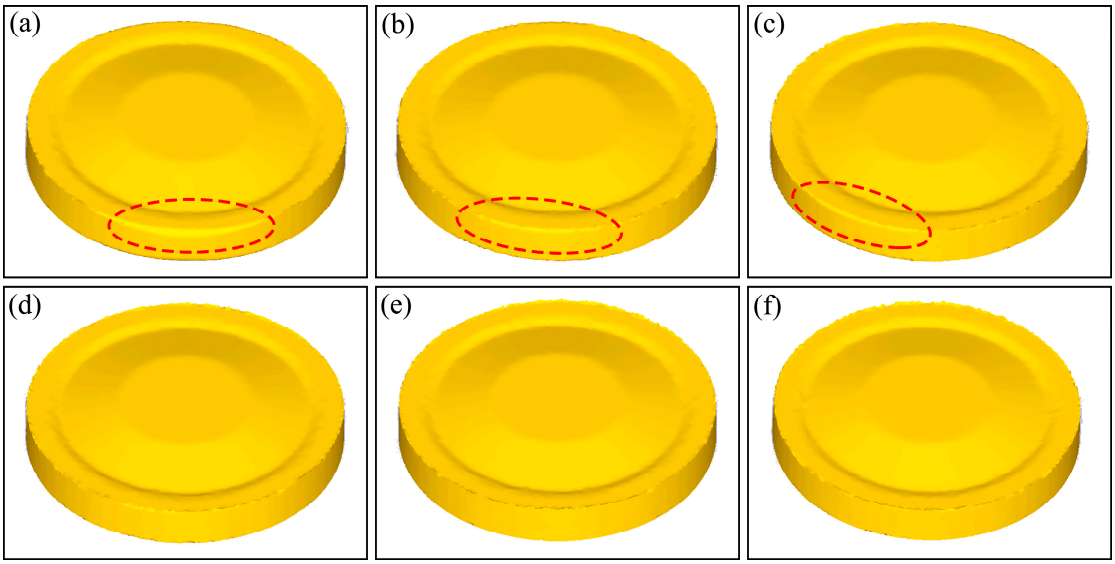

Figure 9. Effect of billet temperature on the filling behavior of the formed parts. (**a**) 1250 °C; (**b**) 1300 °C; (**c**) 1350 °C; (**d**) 1360 °C; (**e**) 1370 °C; (**f**) 1380 °C.

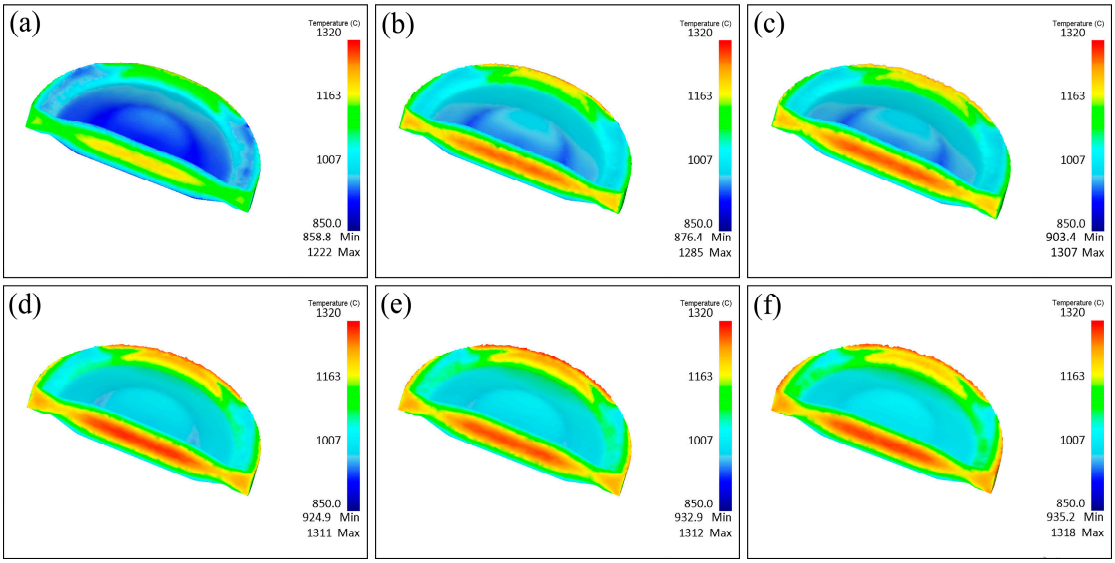

Figure 10. Temperature field distribution of the formed parts with different billet temperatures. (**a**) 1250 °C; (**b**) 1300 °C; (**c**) 1350 °C; (**d**) 1360 °C; (**e**) 1370 °C; (**f**) 1380 °C.

Figure 11 exhibits the distribution of the equivalent stress field of the formed parts with different billet temperatures. It can be found that the equivalent stress at the upper and lower surfaces of the formed parts and at the position of some flanges was high, while the equivalent stress inside the formed part was low. The maximum equivalent stress of the formed part decreased with the increase of the billet temperature, which indicated that the higher the temperature was, the lower the deformation resistance of the billet was. It was conducive to the complete filling of the billet.

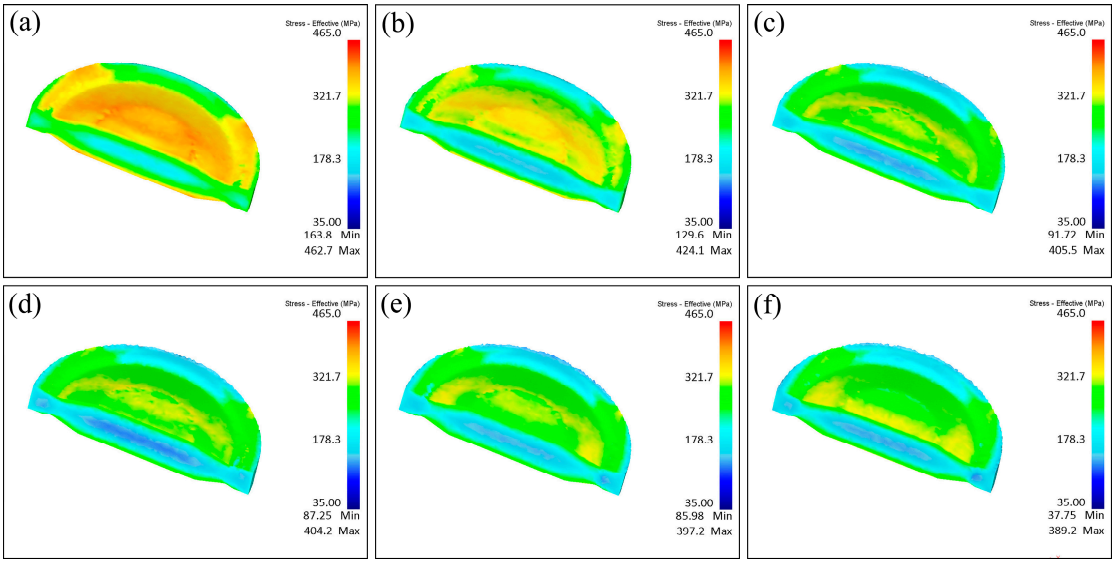

Figure 11. Equivalent stress field distribution of the formed parts with different billet temperatures. (**a**) 1250 °C; (**b**) 1300 °C; (**c**) 1350 °C; (**d**) 1360 °C; (**e**) 1370 °C; (**f**) 1380 °C.

3.3.3. The Effect of Extrusion Velocity on the Results of Numerical Simulation of Thixoforming

Figure 12 shows the temperature field distribution and equivalent stress field distribution of the ejector rod and the temperature field of the formed part with four different extrusion speeds. It can be found that the temperature of the formed part increased with the increase of the extrusion velocity, the equivalent stress of the formed part decreased with the increase of the extrusion velocity, and the temperature of the ejector rod decreased with the increase of the extrusion velocity. With the increase of extrusion velocity, the time of the whole forming process was gradually shortened, so the contact time between the billet and the dies was reduced, and the heat loss of the billet was reduced. Therefore, the temperature of the formed part was higher, and the temperature of the ejector rod was lower. The faster the extrusion velocity was, the higher the temperature of the formed part was. The billet had low deformation resistance at high temperatures, so the equivalent stress of the formed part was reduced accordingly. The simulation results show that the faster the extrusion velocity was, the better the thixoforming effect was. However, due to the coexistence of solid and liquid phases in the semi-solid billet, the solid and liquid phases had different flow speeds during the extrusion process [28], and too fast extrusion speed would lead to severe solid–liquid segregation. Therefore, in order to ensure the smooth filling of the billet in the actual test, it is necessary to select a reasonable extrusion velocity.

3.4. Experimental Verification of the Semi-Solid Thixoforming

Through the numerical simulation results, it was found that the billet placement mode has a great impact on thixoforming. Compared with the billet placed vertically, when the billet was placed horizontally, the contact time of the billet with the dies was shorter. As a result, the temperature of the dies after forming was lower, and the thermal damage to the dies was reduced. When the billet was placed horizontally, the deformation of the billet was smaller, the average equivalent effect change of the formed part was smaller, and the possibility of defects was lower. Therefore, it is more favorable for thixoforming when the billets are placed horizontally. The temperature and extrusion velocity of the billet also have a great influence on thixoforming. The higher the blank temperature is, the lower its deformation resistance is, and the better the blank filling is. The faster the extrusion velocity is, the lower the equivalent stress is. However, higher billet temperature will affect the strength and stiffness of the dies, reducing the service life of the die. High extrusion velocity leads to severe liquid segregation of semi-solid billet and increases the wear and

impact on the dies. Hence, it is necessary to comprehensively consider each parameter and make a reasonable choice in the actual experiment. For this reason, thixoforming experiments of the GH4037 alloy were carried out. During the experiment, different billet temperatures were selected. The temperature of the top die was 400 °C, the temperature of the bottom die, ejector rod was 450 °C, the extrusion velocity was 15 mm/s, and the billet was placed horizontally.

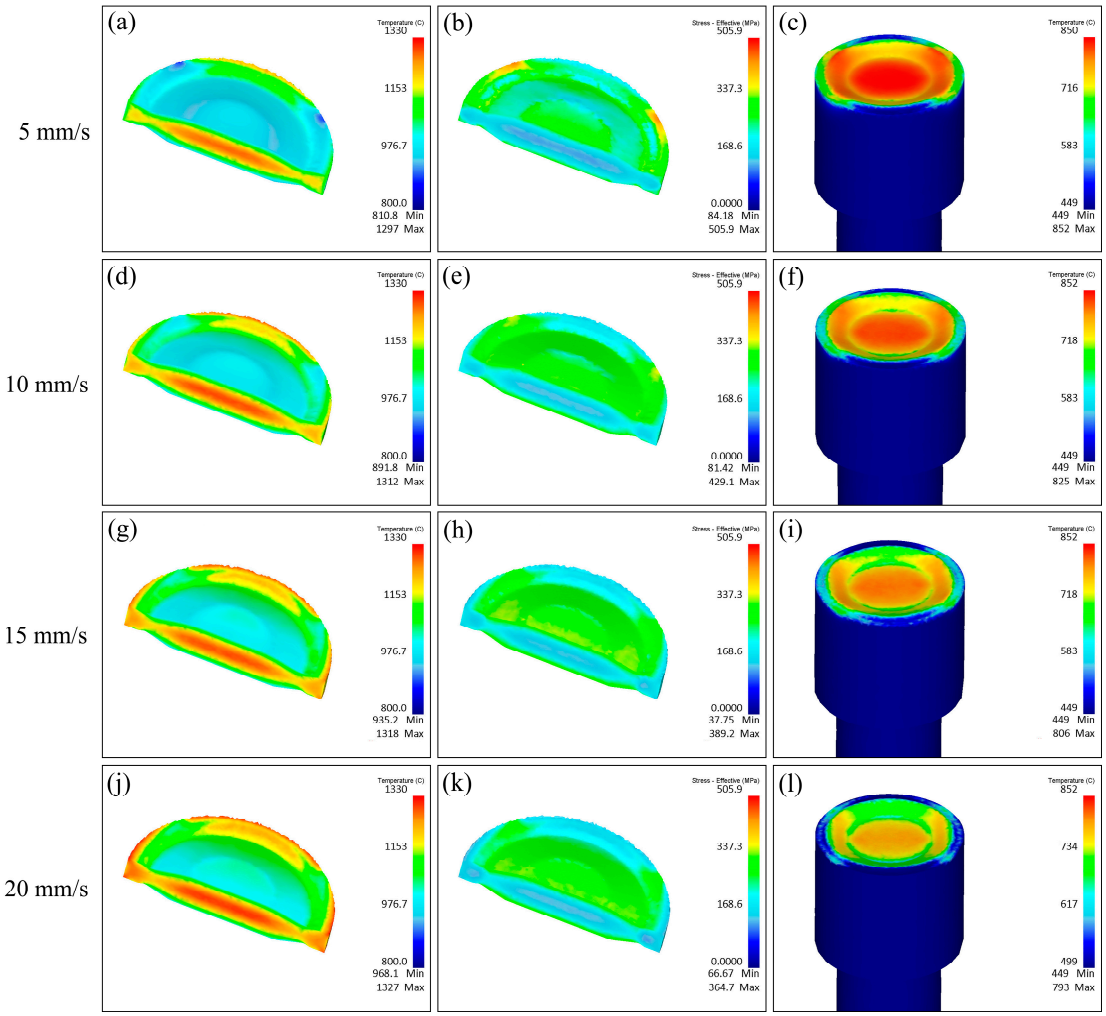

Figure 12. (**a**,**d**,**g**,**j**) The temperature field distribution, (**b**,**e**,**h**,**k**) equivalent stress field distribution of the formed part, and (**c**,**f**,**i**,**l**) the temperature field of the ejector rod with different extrusion speeds.

Figure 13 presents the macro morphologies of the formed parts with different billet temperatures. It was found that when the billet temperature was lower than 1350 °C, cracks appeared at the rim of the formed parts, and the formed parts were not completely filled. When the billet temperature was higher than 1360 °C, the external contour of the formed parts was clear, and the formed parts were completely filled. The experimental results were consistent with the simulation results in Figures 7 and 9, which verified the results of numerical simulation and the feasibility of the semi-solid thixoforming well.

Figure 14 shows the optical microstructures of the formed parts in different locations with different billet temperatures. Location 1 is in the center of the formed part, location 2 is in the transition zone of the half radius of the formed part, and location 3 is at the edge of the formed part. As shown in Figure 14a,b, when the heating temperature was 1320 °C, fine and equiaxed solid grains were clearly observed. Because of the low liquid fraction at 1320 °C, the liquid phases occurred mainly in the form of a liquid band, which was perpendicular to the direction of extrusion. As shown in Figure 14c, the microstructure

consisted of elongated grains and many small recrystallized grains, which presented necklace structures. Furthermore, some pores were observed because the thixoformed part was not fully filled at 1320 °C. As shown in Figure 14d–i, when the heating temperature increased to 1360 °C and 1380 °C, the microstructures of the formed parts consisted of solid grains and liquid phases (including liquid droplet, liquid film, and eutectic phase). At 1380 °C, it was found that the proportion of the liquid phase significantly increased. Meanwhile, it was also observed that, at the same temperature, the microstructure at location 3 had more liquid phases.

Figure 13. Macro morphologies of the formed parts with different billet temperatures.

According to the experimental results, it can be seen that when the billet temperature is low, the proportion of liquid phase in the billet is very small. Therefore, the flow performance of the billet is poor. As a result, holes and cracks may appear at location 3. This is consistent with the numerical simulation results in Figure 7. With the increase of billet temperature, the fraction of liquid phase in the microstructure also increases. Hence, the filling capacity of the billet is significantly improved, resulting in better surface quality of the formed parts. The results in Figures 9 and 13 prove this conclusion. Furthermore, it can be observed that during the forming process, the flow rate of the liquid phase is faster than that of the solid phase. When the billet temperature is high, it may lead to solid–liquid phase segregation. Therefore, it is necessary to select an appropriate billet temperature during the actual forming experiments.

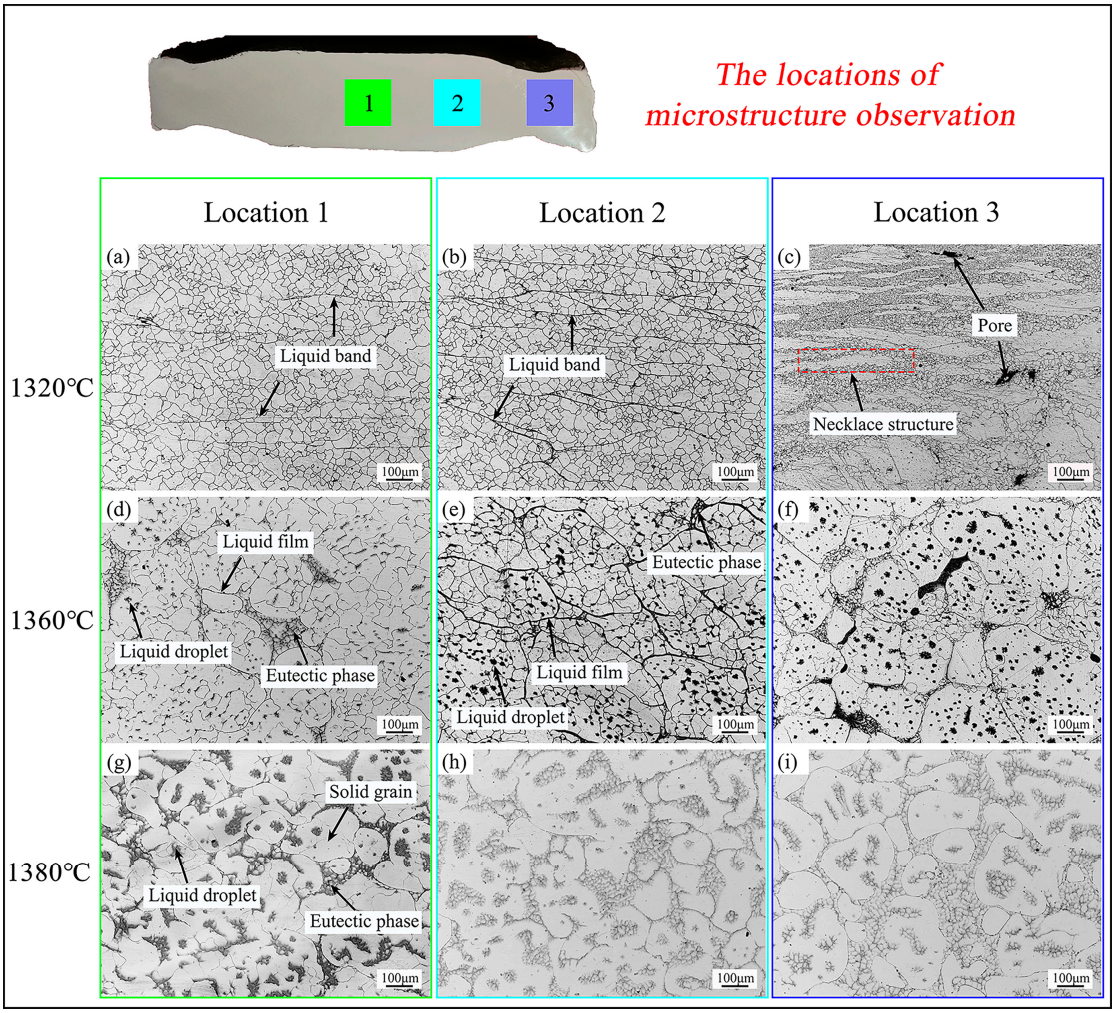

Figure 14. Optical microstructures of the formed parts in different locations with different billet temperatures. (**a**–**c**) 1320 °C; (**d**–**f**) 1360 °C; (**g**–**i**) 1380 °C.

4. Conclusions

In this study, the semi-solid thixoforming of the GH4037 alloy disc-shaped component was simulated. The effects of the billet placement mode, the billet temperature, and the extrusion velocity on the simulation results were analyzed. In addition, thixoforming experiments were carried out, and the experimental results were compared with the numerical simulation results. The main conclusions are as follows:

1. The billet placement mode has a great influence on the numerical simulation results of thixoforming. Compared with the billet placed vertically, when the billet was placed horizontally, the temperature of the dies after forming was lower, the thermal damage to the dies was reduced, and the possibility of defect of the formed parts was lower. Therefore, the horizontal placement of the billet was more conducive to thixoforming.
2. The higher the billet temperature was, the better the alloy-filling was. The faster the extrusion velocity was, the better the thixoforming effect was. However, high billet temperature affected the strength and stiffness of the die, and the high extrusion velocity easily led to the separation of solid and liquid phases of semi-solid billets. Therefore, it is necessary to comprehensively consider each parameter and make a reasonable choice in the actual experiment.
3. The thixoforming experimental results show that when the billet temperature was lower than 1350 °C, the outer edge of the formed part was not filled completely. When the billet temperature was higher than 1360 °C, the formed parts were completely

filled and had good surface qualities. The liquid fraction in the microstructure of formed parts increased with the increase of heating temperature. The liquid fraction at the edge of the formed part was higher than that in the center.

4. The results of the numerical simulation optimized the process parameters for the thixoforming experiment, and the experimental results verified the accuracy of the numerical simulation.

Author Contributions: Conceptualization, J.J.; methodology, G.X.; writing—original draft preparation, G.X.; writing—review and editing, Y.W. and J.J. All authors have read and agreed to the published version of the manuscript.

Funding: This research was funded by The National Natural Science Foundation of China, grant number [51575127]. The authors would like to acknowledge the Original Fund of the Nuclear Power Institute of China, grant number [2023-KJCX-022].

Institutional Review Board Statement: Not applicable.

Informed Consent Statement: Not applicable.

Data Availability Statement: Not applicable.

Conflicts of Interest: The authors declare no conflict of interest.

References

1. Brown, S.B.; Flemings, M.C. Net-shape forming via semi-solid processing. *Adv. Mater. Process.* **1993**, *143*, 36–40.
2. Atkinson, H.V. Semisolid processing of metallic materials. *Mater. Sci. Technol.* **2010**, *26*, 1401–1413. [CrossRef]
3. Wang, L.; Zhang, Z.; Luo, Y.; Xiao, Y.; Tan, F.; Liu, K. Understanding the influencing mechanism of CNTs on the microstructures and wear characterization of semi-solid stir casting Al-Cu-Mg-Si alloys. *Metals* **2022**, *12*, 2171. [CrossRef]
4. Hao, J.; Yu, B.; Bian, J.; Zheng, L.; Nie, S.; Li, R. Comparison of the semisolid squeeze casting and gravity casting process on the precipitation behavior and mechanical properties of the Al-Si-Cu-Mg alloy. *Mater. Charact.* **2021**, *180*, 111404. [CrossRef]
5. Wang, Y.; Liang, X.; Zeng, L.; Wu, H.; Li, H. The microstructure evolution of Al-5Ce alloy prepared by strain-induced melt activation during semi-solid isothermal treatment process. *Mater. Lett.* **2022**, *326*, 132948. [CrossRef]
6. Kim, D.H.; Kim, J.H.; Kobayashi, E. Enhanced mechanical properties of Al-Si-Cu-Mg(-Fe) alloys by a deformation-semisolid extrusion process. *Mater. Sci. Eng. A* **2021**, *825*, 141667. [CrossRef]
7. Cao, L.; Ma, G.; Tang, C. Effects of isothermal process parameters on semisolid microstructure of Mg-8%Al-1%Si alloy. *Trans. Nonferrous Met. Soc.* **2012**, *22*, 2364–2369. [CrossRef]
8. Li, G.; Qu, W.; Luo, M.; Cheng, L.; Guo, C.; Li, X.; Xu, Z.; Hu, X.; Li, D.; Lu, H. Semi-solid processing of aluminum and magnesium alloys: Status, opportunity, and challenge in China. *Trans. Nonferrous Met. Soc.* **2021**, *31*, 3255–3280. [CrossRef]
9. Nie, S.; Gao, B.; Wang, X.; Cao, Z.; Guo, E.; Wang, T. The influence of holding time on the microstructure evolution of Mg–10Zn–6.8Gd–4Y alloy during semi-solid isothermal heat treatment. *Metals* **2019**, *9*, 420. [CrossRef]
10. Zeng, Q.; Zhang, Y.; Li, K.; Zhuang, Y.; Li, J.; Yang, Y.; Yin, D. High-ductility fine-grained Mg-1.92Zn-0.34Y alloy fabricated by semisolid and then hot extrusion. *J. Magnes. Alloys* **2023**, *11*, 533–542. [CrossRef]
11. Chen, Y.; Yuan, Z.; Zhan, H.; Zhao, Y.; Song, X.; Wang, G.; Gu, Y. Unexpected dynamic recrystallization behavior of Ti-7Cu alloy in semi-solid state. *J. Alloys Compd.* **2017**, *712*, 468–476. [CrossRef]
12. Freitas, C.C.D.; Campo, K.N.; Caram, R. Thixoforming of titanium: The microstructure and processability of semisolid Ti-Cu-Fe alloys. *Vacuum* **2020**, *180*, 109567. [CrossRef]
13. Zhao, D.; Chen, Y.; Jiang, C.; Li, Y.; Zhao, Q.; Xu, Y.; Zhan, H.; Wan, M.; Zhao, Y. Morphological evolution of Ti_2Cu in Ti-13Cu-Al alloy after cooling from semi-solid state. *J. Alloys Compd.* **2020**, *848*, 156639. [CrossRef]
14. Liu, W.; Cao, Y.; Guo, Y.; Sun, M.; Xu, B.; Li, D. Solidification microstructure of Cr4Mo4V steel forged in the semi-solid state. *J. Mater. Sci. Technol.* **2020**, *38*, 170–182. [CrossRef]
15. Wang, Y.; Bi, S.; Song, R.; Yanagimoto, J.; Taylor, T. Extremely high temperature carbide precipitation induced intragranular acicular ferrite transformation of M2 steel during semi-solid cooling. *Mater. Lett.* **2022**, *310*, 131516. [CrossRef]
16. Aba-perea, P.E.; Becker, E. Measurement and modeling of thermal evolution during induction heating and thixoforming of low carbon steel. *J. Mater. Process. Technol.* **2020**, *283*, 116717. [CrossRef]
17. Guan, R.; Zhao, Z.; Chao, R.; Lian, C.; Wen, J. Simulation of temperature field and metal flow during continuous semisolid extending extrusion process of 6201 alloy tube. *Trans. Nonferrous Met. Soc.* **2012**, *22*, 1182–1189. [CrossRef]
18. Koeune, R.; Ponthot, J.P. A one phase thermomechanical model for the numerical simulation of semi-solid material behavior. Application to thixoforming. *Int. J. Plasticity* **2014**, *58*, 120–153. [CrossRef]
19. Zhu, G.; Xu, J.; Zhang, Z.; Liu, G. Numerical simulation of die filling behavior of AZ91D in the semisolid process. *China Foundry* **2010**, *7*, 127–131.

20. Seo, P.K.; Kim, H.C.; Kang, C.G. Numerical integration design process to development of suspension parts by semi-solid die casting process. *J. Mater. Process. Technol.* **2007**, *183*, 18–32. [CrossRef]
21. Ma, Z.; Zhang, H.; Fu, H.; Yang, Y.; Wang, J.; Du, M.; Zhang, H. Insights into the rheological modeling of semi-solid metals: Theoretical and simulation study. *J. Mater. Sci. Technol.* **2022**, *100*, 182–192. [CrossRef]
22. Lin, B.; Fan, T.; Li, H.; Zhao, Y.; Zhang, W.; Liu, K. Microstructure and high temperature tensile properties of Al-Si-Cu-Mn-Fe alloys prepared by semi-solid thixoforming. *Trans. Nonferrous Met. Soc.* **2021**, *31*, 2232–2249. [CrossRef]
23. Rassili, A.; Atkinson, H.V. A review on steel thixoforming. *Trans. Nonferrous Met. Soc.* **2010**, *20*, s1048–s1054. [CrossRef]
24. Pierret, J.C.; Rassili, A.; Vaneetveld, G.; Lecomte-Beckers, J. Stability of steel thixoforming process. *Trans. Nonferrous Met. Soc.* **2010**, *20*, s937–s942. [CrossRef]
25. Wang, P.; Cui, J.; Lu, G. Semi-solid thixoforming simulation of Al-Cu-Mn-Ti alloy parts via AnyCasting. *J. Mater. Sci. Technol.* **2007**, *3*, 75–78.
26. Tong, J.; Ding, X.; Wang, M.; Yagi, K.; Zheng, Y.; Feng, Q. Assessment of service induced degradation of microstructure and properties in turbine blades made of GH4037 alloy. *J. Alloys Compd.* **2016**, *657*, 777–786. [CrossRef]
27. Jiang, J.; Xiao, G.; Wang, Y.; Liu, Y.; Zhang, Y. High temperature deformation behavior and microstructure evolution of wrought nickel-based superalloy GH4037 in solid and semi-solid states. *Trans. Nonferrous Met. Soc.* **2020**, *30*, 710–726. [CrossRef]
28. Chen, G.; Chen, Q.; Qin, J.; Du, Z. Effect of compound loading on microstructures and mechanical properties of 7075 aluminum alloy after severe thixoformation. *J. Mater. Process. Technol.* **2016**, *229*, 467–474. [CrossRef]